Mechanistic Investigation and Free Energies of the Reactive Adsorption of Ethanol at the Alumina/Water Interface

Jérôme Rey, Paul Clabaut, Romain Réocreux, Stephan Steinmann, Carine Michel

Mechanistic investigation and free energies of the reactive adsorption of ethanol at the alumina/water interface

Jérôme Rey,[†] Paul Clabaut,[†] Romain Réocreux,[‡] Stephan N. Steinmann,[†] and Carine Michel[*,†]

†*ENS de Lyon, CNRS UMR 5182, Laboratoire de Chimie, F69342, Lyon, France*

‡*Thomas Young Centre and Department of Chemical Engineering, University College London, Roberts Building, Torrington Place, London WC1E 7JE, United Kingdom*

E-mail: carine.michel@ens-lyon.fr

Abstract

Controlling the adsorption/desorption of molecules at the solid/water interface is central to a wide range of fields from catalysis to batteries. For instance, adsorbing alcohols at the surface of γ-Al_2O_3 can prevent its chemical weathering. To make sure that γ-Al_2O_3 remains a stable catalyst support under operating conditions in liquid water, it is crucial to design alcohols that cannot desorb easily. Taking ethanol as a typical example, we here compare the adsorption/desorption mechanism for two distinct adsorption modes of ethanol at the water/alumina interface using various DFT-based approaches. Thermodynamic integration simulations unambiguously identify ethoxy as the more stable adsorption mode. The presence of liquid water yields to adsorption barriers of at least 20 kJ·mol^{-1}. To better assess the effect of water, we perform 3D well-tempered metadynamics simulations

that include a bias accounting for solvation effects and proton transfers at the interface. Activating the proton shuffling allows to explore a variety of protonation and hydration configurations and yields to higher barriers (up to 40 kJ·mol^{-1}) than the ones predicted by thermodynamic integration where the solvent reorganisation was assumed to be decoupled from the desorption. This study illustrates the importance of treating explicitly solvation effects when modelling reactions at the solid/liquid interface.

1 Introduction

Adsorption/desorption processes at the solid/water interface play a key role in tribology,[1] heterogeneous catalysis,[2] electrochemistry,[3,4] chromatography, *etc*. The small volume of the interfacial region relative to that of the liquid and the solid phases makes experimental investigations challenging.[5–7] Available information about water structuration at such interfaces are therefore limited to very specific conditions, such as thin water layers under high-vacuum conditions (obtained *via* spectroscopy[8,9] or microscopy[7]) or under applied electric potentials.[10] Additional complexity arises from water being able to dissociate upon chemisorption onto metals,[11] oxides,[12] and other materials.[13] Moreover the liquid structure of water is believed to depend on the nature and the morphology of the surface.[5,7] Atomistic modelling therefore appears as a complementary tool of choice to gain detailed understanding beyond spectroscopic signatures and has been extensively applied to the study of the structuration of interfacial water,[7] and the adsorption of molecules or ions at the solid/water interface.[14,15]

Modelling a solid/water interface requires an extensive sampling of the phase space of the liquid phase.[16] In most cases, the dynamics of water is slowed down at the interface by several orders of magnitude, making the sampling of such interfacial system challenging.[17] Non-reactive adsorptions can be treated efficiently with molecular mechanics (MM) .[14,18,19] Combining MM with an *ab initio* description of the surface/adsorbate interactions provides

a reliable description of the energetics of adsorption.[20–24] For instance, using our recent MMSolv approach, we have been able to predict semi-quantitatively the adsorption energies of phenol and benzene at the water/Pt interface.[25] This hybrid scheme has highlighted the significance of surface desolvation as a limiting process to the adsorption of molecules on metal surfaces. Reactive adsorptions are more challenging to investigate: on top of the aforementioned changes in solvation, reactions involving the solvent, the adsorbates and/or the surface also occur during the adsorption process. Typically, proton-shuffling between water, the adsorbate (*e.g.*, an alcohol) and the surface (*e.g.*, an oxide) are likely to concur with the adsorption of protic molecules.[26] Therefore, accounting for proton transfers can be crucial when studying reactive adsorptions. Reactive force fields[27–29] or semi-empirical methods such as DFTB[30,31] appear as good strategies as they offer the possibility to sample the phase-space along reaction-coordinates at reasonable costs. More recently, force fields based on machine learning techniques, such as neural networks, have also been successfully developed to investigate solid/liquid interfaces.[32–34] However these methods fail at handling increased numbers of atom types. More generally, empirical methods for the study of reactive adsorptions require the development of *ad hoc* system-specific parameters. This represents a severe limitation that can be overcome moving to Density Functional Theory (DFT). Investigating reactions at the solid/water interface using DFT can be performed by biasing *ab initio* molecular dynamics along selected collective variables. Metadynamics,[35–38] umbrella sampling[39] and thermodynamic integration[40,41] are the most common such methods. Combining different theoretical methods has proved to provide a better understanding of the mechanisms in complex environments and in presence of water.[42,43] Using *ab initio* metadynamics, we have recently investigated the mechanism of the hydrolysis of γ-Al_2O_3, an important support in heterogeneous catalysis, when it is immersed in water. Experimentally it is found that certain polyols act as protecting additives against the hydrolysis of the support.[44] We have shed light on the role of the adsorption of some polyols at the γ-Al_2O_3/water interface in preventing the hydrolysis.[45]

Although there is evidence that alcohols chemisorb on γ-Al_2O_3,[45–47] the details of the adsorption sites and energetics are yet to be elucidated. The limited understanding of the adsorption process of alcohols at the γ-Al_2O_3/water interface makes the quest of better protecting additives empirical.

Herein, we investigate the adsorption of ethanol, taken as a typical alcohol, at the γ-Al_2O_3/water interface combining three simulation methods to unravel the mechanism of adsorption at this complex interface and the relative stability of two adsorption modes. First, we estimate reaction free energies using a static approach combined with different models accounting for solvation. Then, we refine the energetics of the different processes using *ab initio* thermodynamic integration. Last, we explore in more details the adsorption mechanism using *ab initio* metadynamics to build free energy surfaces in three dimensions, including a collective variable describing solvation effects.

2 Computational details

2.1 Models of the γ-Al_2O_3/water interface

Our model of the γ-Al_2O_3(110)/water interface was taken as the last frame of the ab initio molecular dynamics (AIMD) trajectory we published previously.[17] To study the chemisorption of ethanol at the γ-Al_2O_3(110)/water interface, one chemisorbed water is subtituted by ethanol (see Figure 1 a)). Briefly, a periodic slab of the γ-Al_2O_3(110) surface of 10 Å thickness was cleaved using the bulk model of γ-Al_2O_3 proposed by Krokidis *et al* ($Al_{128}O_{192}$).[48] Then, we hydrated the top surface[49] of a p(2x2) cell and took into account the water-induced surface reconstruction evidenced by Wischert et al.[50] We put the obtained hydrated surface in contact with a slab of liquid water of 20 Å (163 H_2O). The periodic images perpendicular to the interface were separated by a void of 10 Å.

Proton transfers were observed at the interface during the trajectory of 74 ps (including equilibration). The surface state of the resulting p(2x2) cell of S_{ref} is represented schemati-

cally in Figure 1 b). The original primitive cell (highlighted with a square) exposes two octahedral aluminium atoms ((1) and (2) following Copeland's denomination[46]) and two tetrahedral aluminium atoms (α and β) at the surface. In the p(2x2) cell, 20 water molecules are chemisorbed, completing the aluminium coordination up to 4 or 6 depending on the sites. 13 of these water molecules are dissociated, generating 26 hydroxyl groups at the surface. Initial structures can be found in Supporting Information.

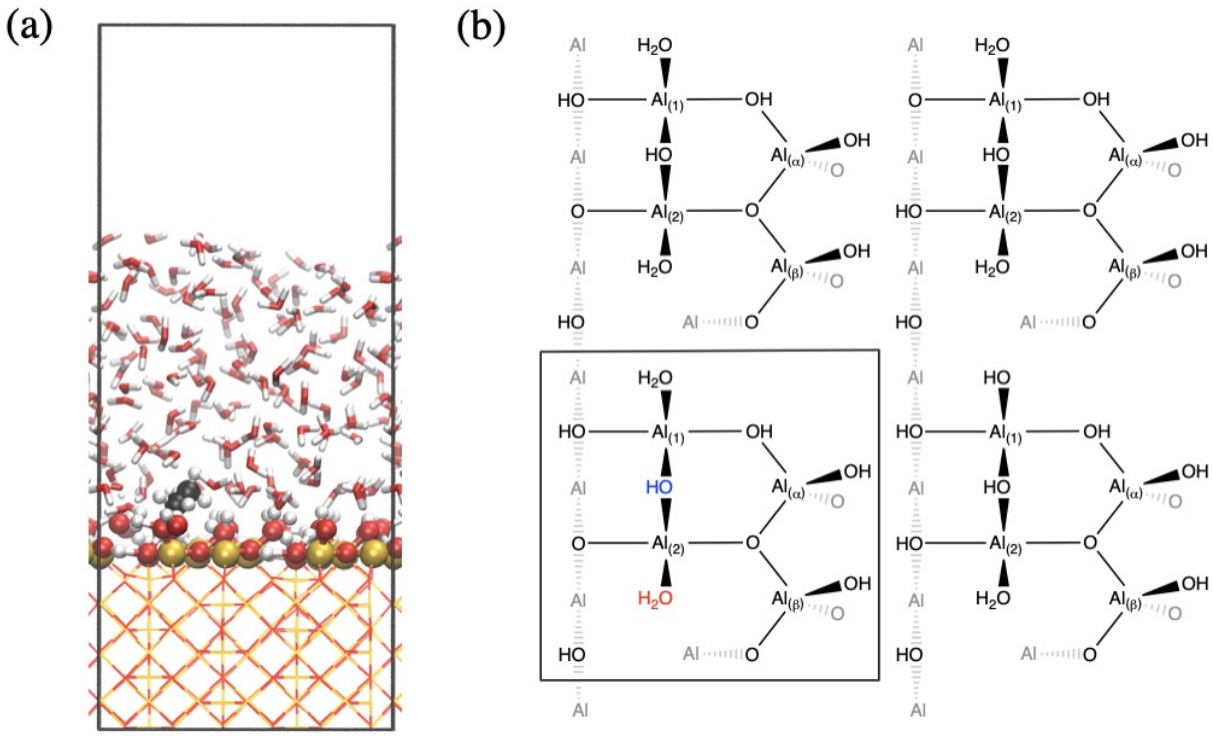

Figure 1: (a) Ethanol chemisorbed at the γ-Al_2O_3(110) surface/water interface (μ_1) (b) Schematic representation of the hydrated γ-Al_2O_3(110) surface. This surface is used as a reference (S_{ref}) when computing thermal balances. It is also used to build the initial γ-Al_2O_3(110)/water interface. μ_1 is obtained by substituting the water shown in red by ethanol. μ_2 is obtained by substituting the OH shown in blue by ethoxy. The original elementary cell used for the construction of the p(2x2) supercell is shown as a black box.

2.2 Desorption/Adsorption of ethanol at the γ-Al_2O_3/water interface

We have studied the desorption of ethanol from γ-Al_2O_3(110) to liquid water considering two configurations of ethanol that differ by their number of $Al-O_{ethanol}$ bonds (see Figure 1 and S1). This number of bonds is later referred to as *multiplicity*. In analogy with coordination chemistry, when the *multiplicity* is 1 or 2, the configuration is named μ_1 or μ_2 respectively. By extension, μ_0 refers to ethanol desorbed in the bulk of the water slab. In the μ_1 configuration (shown in Figure 1 a)), ethanol interacts through its oxygen with one aluminium atom of the surface, namely the octahedral $Al_{(2)}$, thereby substituting a non-dissociated water molecule (shown in red in Figure 1 b)). In the μ_2 configuration, ethanol is dissociated, bridging two aluminium atoms ($Al_{(1)}$ and $Al_{(2)}$). It replaces the hydroxyl group that bridges the two aluminium atoms (shown in blue in Figure 1 b)).

2.3 General parameters for static DFT computations with VASP

For the static DFT calculations, electronic energies are computed using the plane-wave VASP 5.4.1 code.[51,52] The PBE functional is used to describe electron interactions,[53,54] supplemented by the dDsC dispersion correction.[55,56] The electron-ion interactions are described by the PAW formalism.[57,58] The plane-wave energy cutoff is set to 400 eV. This choice is made to be compatible with our implementation of the MMSolv method (details in the next section).

For the implicit solvent computations, the Polarisable Continuum Model (PCM) implemented in the VASPsol module[59] is used. The default settings for cavitation energy are used.

The entropy of adsorption is estimated neglecting all vibrational contributions. The entropy of adsorbates is therefore completely neglected (as they do not rotate or translate freely). Thus, the entropy of adsorption writes:

$$\Delta_{ads}S = -S_{aq}(\mathrm{EtOH}) + S_{aq}(\mathrm{H_2O}) \tag{1}$$

where $S_{aq}(\mathrm{EtOH})$ and $S_{aq}(\mathrm{H_2O})$ are the entropies (limited to the translational and rotational contribution) of solvated ethanol and solvated water. We have used the experimental value for the entropy of a solvated water molecule and we have estimated the entropy of solvated ethanol using the empirical relationship ($S_{gas}(EtOH)$ is the gas phase entropy of ethanol) established by Wertz and co-workers:[60]

$$S_{aq}(EtOH) = 0.54 \cdot S_{gas}(EtOH) + 2.76 \cdot 10^{-2} (\mathrm{kJ \cdot mol^{-1} \cdot K^{-1}}) \tag{2}$$

2.4 Molecular mechanics computations with AMBER

The MMSolv computations have been conducted using the method and workflow described in our previous work for the evaluation of the adsorption free energy of benzene or phenol on a Pt(111) surface.[25] The γ-alumina slab is frozen. The Lennard-Jones parameters for γ-alumina atoms are taken from the CLAYFF forcefield.[61] Chemisorbed water molecules (dissociated or not) are also frozen. Their Lennard-Jones parameters are taken from the UFF forcefield,[62] and their partial charges are extracted from DFT static computations of the hydrated slab, following our previously described MMSolv method.[25]

2.5 Biased AIMD

2.5.1 General parameters

Energies and forces are computed using the CP2K-Quickstep[63–66] implementation of DFT with the Gaussian Plane Wave (GPW) approach, combining a MOLOPT double-ζ basis set (DZVP) and an auxiliary plane waves basis set with a 400 Ry cutoff for valence density. Goedecker-Teter-Hutter (GTH) pseudo-potentials[67–69] are used to replace the core electrons. The Perdew-Burke-Ernzerhof (PBE) functional[54] is supplemented by Grimme's D3 correction.[70] The self-consistent field convergence criterion is set to $5 \cdot 10^{-6}$ Hartree.

Dynamic samplings are performed in the NVT thermodynamic ensemble, controlling

the temperature at 330 K *via* the Canonical Sampling through Velocity Rescaling (CSVR) thermostat.[71] The two bottom-most layers of alumina are frozen. An integration time step of 0.5 fs is chosen for runs associated with thermodynamic integration, while 1 fs is used for metadynamics runs, for which we have considered a threefold increase of atomic weight for hydrogen in order to improve the efficiency of the sampling. Since position-dependent observables are independent of the atomic masses once convergence is achieved, this choice does not influence the resulting energies.[72]

2.5.2 Thermodynamic integration

The *height* of ethanol (noted CV_{height}) is defined as the absolute coordinate of the oxygen atom of ethanol in the out-of-plane direction. The first 5 ps of each run are considered as equilibration and thus discarded for analysis, leaving production trajectories of at least 10 ps each. In total, 256.4 ps have been accumulated for the desorption of μ_1 (Table S1) and 304.5 ps for the desorption of μ_2 (Table S2). We assumed here that changes in hydration are fast and decoupled from the adsorption/desorption process. Hence, at $CV_{height} \geq 13$ Å, we carefully checked that the water reorganisation was fast enough to complete the hydration of the alumina surface. In particular, we had to bring a water molecule close to the surface using a slow growth simulation for μ_1 desorption. At $CV_{height} > 14$ Å, the configurations of the two TI runs correspond to a free ethanol molecule in liquid water, and only the free energy profile corresponding to the TI run starting from μ_2 is used.

2.5.3 Well-tempered metadynamics

Two well-tempered metadynamics[73] simulations have been carried out using the open-source, community-developed PLUMED library,[74] version 2.4.2.[75] The first one starts from μ_1 and the other one starts from μ_2. The bias potential is constructed by adding Gaussian hills (initial height of 3.3 kJ·mol^{-1}, bias factor of 100 and temperature of 330 K) every 10 fs in the space described by three collective variables (CVs). To accelerate the exploration,

four walkers[76] have been used starting from four structures with the ethanol located at different CV_{height}. The simulations are stopped after several recrossing of the transition zones and a decrease in the gaussian height of at least 25 % in the minima. This has required 20,463 gaussians (204.6 ps) for the desorption of μ_1 and 26,878 gaussians (268.8 ps) for the desorption of ${}_m u_2$. Noticeably, while a 3D phase-space is rebuilt, the computational burden is not increased compared to TI.

The set of collective variables for biasing the desorption of μ_1 and $\mu 2$ is chosen to be as close as possible but is adapted to the specificities of those two adsorption modes:

- The *height* (CV_{height}) is defined just like in the TI. The width of the Gaussian hills along this CV was set to 0.04 Å.

- The *multiplicity* (CV_{multi}) is defined as the coordination number between the oxygen atom of ethanol and the aluminium atoms of the surface: $\mathrm{Al}_{(2)}$ for the metadynamics starting from μ_1 (see Fig. 1 b)); and $\mathrm{Al}_{(1)}$ and $\mathrm{Al}_{(2)}$ for the metadynamics starting from μ_2 (see Fig. 1 b)). The width of the Gaussian hills along this CV is set to 0.04.

- The *solvation* (CV_{solv}) is designed to account for the changes in solvation of ethanol and alumina upon desorption. These changes are described through the number of hydrogen bonds between the water solvent and the hydroxyl group of ethanol and the number of $\mathrm{Al{-}O_{water}}$ bonds. CV_{solv} is thus defined as follow:

$$CV_{solv} = CN(O_{ethanol}; H_{water} \cup H_{ethanol}) + CN(H_{ethanol}; O_{water} \cup O_{ethanol}) + CN(Al_{(n)}; O_{water}) \tag{3}$$

where $CN(A;B)$ stands for the coordination number between two groups of atoms (A and B). $O_{ethanol}$ corresponds to the oxygen of ethanol. H_{water} and O_{water} include all hydrogen atoms and all oxygen atoms that originate from water molecules (free, adsorbed, or dissociated). $H_{ethanol}$ stands for the hydrogen atom of the hydroxyl group of ethanol and is therefore defined only for the simulations starting with μ_1.

$Al_{(n)}$ stands for the aluminium atoms that are bonded to ethanol, i.e., $Al_{(2)}$ when starting with the μ_1-ethanol, and $Al_{(1)}$ and $Al_{(2)}$ when starting with the μ_2 (see Figure 1 b)). The width of the Gaussian hills along this CV was also set to 0.04.

The coordination numbers between two groups of atoms A and B used in Eq. 3 were defined following the PLUMED implementation:[75]

$$CN(A;B) = \sum_{i \in A} \sum_{j \in B} s_{ij} \tag{4}$$

with

$$s_{ij} = \begin{cases} \frac{1-\left(\frac{r_{ij}-d_0}{r_0}\right)^n}{1-\left(\frac{r_{ij}-d_0}{r_0}\right)^m} & \text{if } r > d_0 \\ 1 & \text{if } r < d_0 \end{cases} \tag{5}$$

with r_{ij} the distance between the atoms i and j, and the d_0 and r_0 two cut-off distances chosen as presented in Table 1.

Table 1: Numerical parameters used to define the coordination numbers between atoms.

type	d_0 (Å)	r_0 (Å)	n	m
O ; H	1.9	0.4	4	10
Al ; O	1.9	0.8	4	10

2.5.4 Computing free energy differences between macro-states

To compare the results of the thermodynamic integration (with only a bias along one variable), and the well-tempered metadynamics simulations (three variables), it is necessary to integrate the free energy landscapes over the different microstates (visited during the simulation) that belong to the same macro-state. The free energy differences between two macro-states of respective populations p_1 and p_2 and defined by the boundaries ($[CV_{1,min};CV_{1,max}]$...$[CV_{N,min};CV_{N,max}]$) (with N the number of CVs) is given by the following formulae:

$$\Delta F = -RT \cdot \ln\left(\frac{p_1}{p_2}\right) \tag{6}$$

where p_1 and p_2 are defined as follows:

$$p(CV_{i,min}, CV_{i,max}, i = 1..N_{CV}) = \frac{1}{K} \int_{CV_{1,min}}^{CV_{1,max}} \cdots \int_{CV_{N,min}}^{CV_{N,max}} \exp\left(-\frac{F(x^N_{CV})}{RT}\right) dx^N_{CV} \tag{7}$$

The integration variable x^N_{CV} is the coordinate of the system in the N-space defined by the CVs and K a normalization constant. Integration is performed using PLUMED.[74]

3 Results and discussion

To investigate the mechanism of adsorption/desorption of ethanol at the γ-Al_2O_3(110)/water interface , we compare two configurations: (i) in μ_1, the ethanol molecule is chemisorbed interacting with a single aluminium atom (Figure 1 a)) ; (ii) in μ_2, the ethanol molecule is adsorbed dissociatively and bridges two aluminium atoms (Figure 1 b)) . More details are provided in section 2.1 and 2.2. In the desorbed state (μ_0), ethanol is solvated in bulk water.

We have considered three approaches of increasing complexity aiming at identifying the role of the water environment on the adsorption/desorption of ethanol. First, static models provides a first insight on the relative stability of the three states under consideration (μ_0, μ_1, μ_2). Then, the barrier of desorption is estimated using *ab initio* thermodynamic integration (TI) using the height as a proxy for the reaction coordinate (CV_{height}). Last, *ab initio* metadynamics allows to explicitly include a bias in solvation (CV_{solv}) to sample proton transfers but also accelerate the EtOH/water exchange through a biasing potential.

3.1 Static approaches and classical solvation

Free energy differences are computed based on the following substitution reaction:

$$EtOH + H_2O@Al_2O_3 \longrightarrow EtOH@Al_2O_3 + H_2O \quad (8)$$

We have screened several possible orientations of chemisorbed water molecules and hydroxyl as well as several surface proton configurations for μ_1 and μ_2 using geometry optimisations. The most stable structures are shown in Figure S1. The free energy diagram including the two most stable OH/H surface configurations for each each case is presented in Figure 2. Three situations are compared: (a) in absence of solvent (b) using a polarisable continuum model (PCM) for the water solvent and (c) using a hybrid approach (MMSolv) to explicitly include the effect of solvating water molecules.

When solvation is not accounted for (Figure 2 (a)), the non-dissociative adsorption to μ_1 is almost athermic ($\Delta F_{ads}(\mu_1) = -1$ kJ·mol^{-1}) whereas the dissociative adsorption to μ_2 is exothermic ($\Delta F_{ads}(\mu_2) = -13$ kJ·mol^{-1}).

Upon the addition of solvent effects using PCM (Figure 2 (b)), each adsorbed state is systematically stabilised, but this stabilisation depends on the adsorption mode and the localisation of the protons, spanning -3 kJ·mol^{-1} to -20 kJ·mol^{-1}. Noticeably, the relative energies of the two considered adsorption modes is inverted, μ_1 being more stable than μ_2.

Although implicit solvation is well-suited to describe indirect solvation effects like modifications in the long-range electrostatic interactions, it cannot provide a proper estimate of other significant contributions, such as the rearrangement of the hydrogen bonding network.[77–79] To overcome this problem, we move to the explicit solvation method MMSolv,[25] an hybrid approach that we have recently developed. It proceeds by freezing the surface and adsorbate in a given geometry and performing an extensive sampling of the water phase *via* molecular mechanics in order to determine how the solvation varies between two states using an alchemical transformation. The inclusion of the explicit solvation modifies

in a contrasted manner the relative stability of the adsorption modes as depicted in Figure 2 (c). The μ_1 adsorption mode is destabilised compared with the PCM results while μ_2 is stabilised. As a result, the bridging adsorption mode μ_2 is found to be the most stable, with an adsorption free energy of -23 kJ·mol^{-1}.

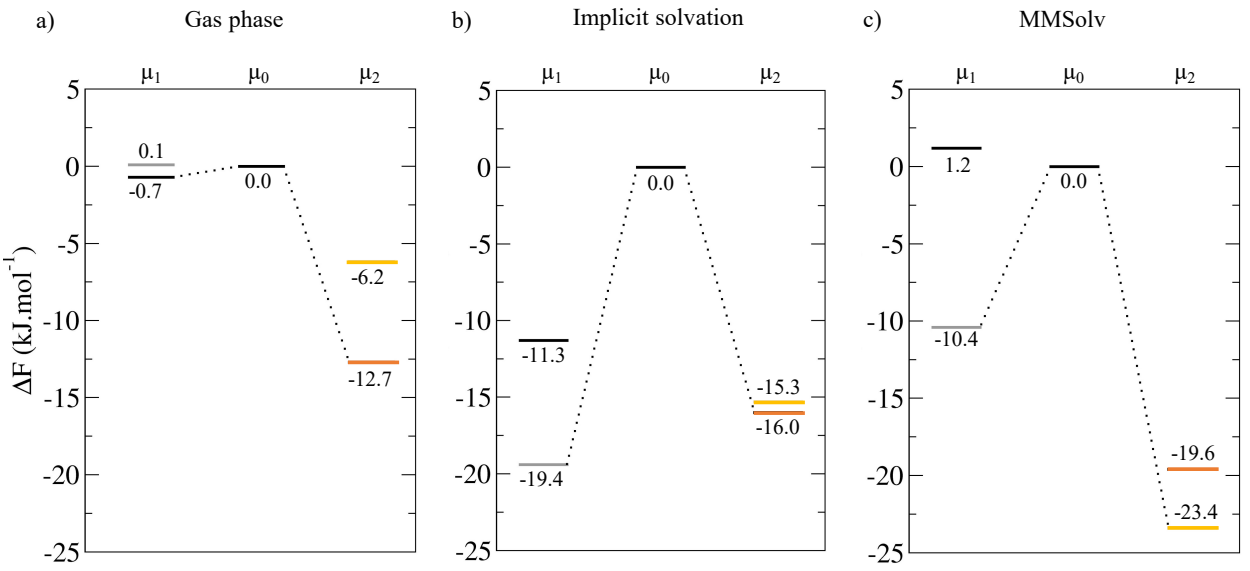

Figure 2: Free energy diagram of the adsorption of ethanol at the γ-Al_2O_3(110)/water interface. In (a), the bulk water solvent is neglected while it is included in (b) by using a polarisable continuum model and in (c) using the hybrid scheme MMSolv.[25] The results for the two best configurations for each case are shown. Each colour corresponds to a given configuration and orientation of surface protons. All free energies are given in kJ·mol^{-1} relatively to S_{ref} (see Figure 1)

3.2 Thermodynamic Integration

Thermodynamic integration (TI) has used to determine the activation barrier associated with the adsorption/desorption of ethanol. The free energy profiles along the *height* (CV_{height}, see 2.5.2) are computed starting from μ_1 and μ_2. As shown in Figure 3, the two profiles present a maximum around CV_{height}=12.5 Å. The transition state lies in a partially structured region of the liquid phase previously identified as the physisorbed layer.[17] Since the two systems become chemically equivalent above 14 Å (desorbed ethanol, also referred to as μ_0), we have merged the tails of the different profiles.

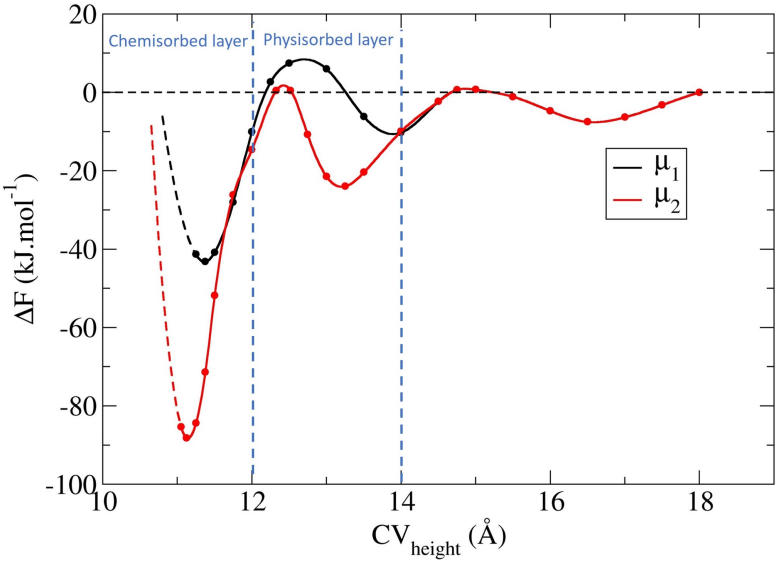

Figure 3: Free energy profiles ΔF as a function of CV_{height} computed with thermodynamic integration starting from μ_2 and μ_1 respectively. The dashed parts of the profiles represent an extrapolation at small displacement along CV_{height} determined by a quadratic fit. The profiles are merged for $CV_{height} > 14$ Å as explained in the computational details. The light blue vertical lines represent the limit of the structured water layers of water evidenced on this interface by Réocreux et al.[17]

Using μ_0 as a common free energy reference, the two profiles give access to the relative stability of μ_1 and μ_2 as well as the barriers of adsorption and desorption, applying Equations 6 and 7. The dissociative adsorption mode μ_2 is the most stable one ($\Delta F_{ads}(\mu_1) = -32$ kJ·mol^{-1} vs. $\Delta F_{ads}(\mu_2) = -61$ kJ·mol^{-1}), in qualitative agreement with the static

calculations using the MMSolv approach for solvation. The related adsorption barrier is slightly lower to reach μ_1 than to reach μ_2 (19 kJ·mol^{-1} vs. 28 kJ·mol^{-1}). Noticebly, the bridging ethoxy in μ_2 is protonated to ethanol very early in the desorption process (before the transition state, $CV_{height} < 12.5$ Å) and no minimum associated to a μ_1 configuration could be identified since the number of Al$-$O$_{\text{ethanol}}$ bonds (also called *multiplicity*) drops abruptly from 2 to 0 (see Figure S2).

In both cases (μ_1 and μ_2), the solvation (as defined by CV_{solv}) increases strongly after desorption, through the hydration of the two aluminium atoms, with one or two additional Al$-$O$_{\text{water}}$ bonds, and through the hydration of ethanol, forming 1 or 2 hydrogen bonds with water (see the supplementary information for a detailed analysis).

3.3 *ab initio* well-tempered metadynamics

The TI simulations have demonstrated that accounting for explicit solvation is associated with barriers of roughly 20 kJ·mol^{-1} to adsorb ethanol at the alumina/water interface. The change in *solvation* along this process is likely to be critical in addition to the change in *height*. To sample the phase-space using more than one collective variable, we have used *ab initio* well-tempered metadynamics. This change in *solvation* is accounted for using CV_{solv}. This collective variable drives the solvation of ethanol but also the hydration of the vacant coordination site(s) at the alumina surface created during the ethanol desorption. Similarly to the TI, the height of ethanol (CV_{height}) is used to drive the desorption of ethanol from the γ-Al_2O_3(110)/water interface to bulk water. Last, to clearly distinguish between μ_0, μ_1 and μ_2 states, it is also necessary to include the number of bonds of ethanol to the alumina surface (*multiplicity*, CV_{multi}). Details about the *ab initio* well-tempered metadynamics simulations can be found in Section 2.5.3.

Starting from chemisorbed ethanol μ_1, we have obtained the free energy surface FES_1 represented in Figure 4. The phase-space corresponding to μ_1 ($CV_{multi} > 0.5$) is small in volume: 10.5 Å$< CV_{height} <$ 12.5 Å. It includes four minima corresponding to four different

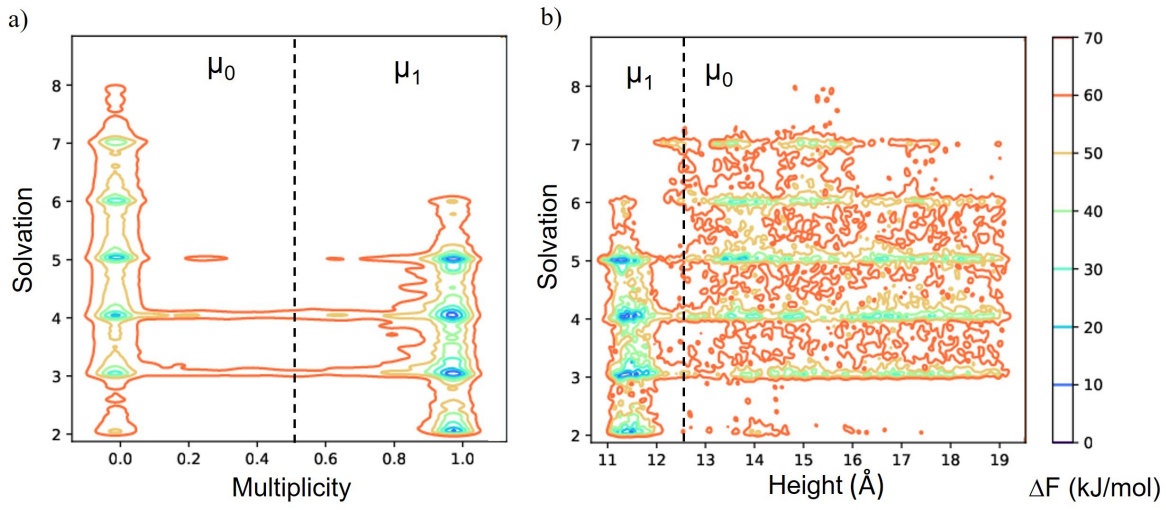

Figure 4: 2D representations of the free energy surface FES_1 built using well-tempered metadynamics including the μ_1 adsorption mode of ethanol at the γ-Al_2O_3(110)/water interface. **(a)** FES_1 as a function of CV_{multi} and CV_{solv} **(b)** FES_1 as a function of CV_{height} and CV_{solv}. The μ_0 macro-state ($CV_{multi} < 0.5$, $CV_{height} > 12.5$ Å, desorbed ethanol) and the μ_1 macro-state ($CV_{multi} > 0.5$, $CV_{height} > 12.5$ Å, chemisorbed ethanol) are separated by a dash line. The third collective variable has been integrated out using the PLUMED library.[74]

solvation states (CV_{solv}=2,3,4,5), which encompass a variety of structures including proton exchanges between ethanol, the chemisorbed water molecules and the surrounding water molecules. In contrast, the portion associated to μ_0 ($CV_{multi} > 0.5$) is large, covering the whole volume of the available liquid (12.5 Å < CV_{height} < 19 Å). Sampling this large volume has required several walkers in the well-tempered metadynamics to obtain a semi-quantitative estimation of adsorption free energy, $\Delta F_{ads} = -14$ kJ·mol^{-1}, applying Equations 6 and 7 (see Figure S3 a) for the 1D profile along CV_{multi}). The transition state region is located around $CV_{multi} = 0.5$ as expected, with a free energy barrier of adsorption of 36 kJ·mol^{-1}.

The lowest transition channel is located at $CV_{solv} = 4$. Since the deepest well of the μ_0 state is found at $CV_{solv} = 5$, the adsorption mechanism is a two-step process: (i) desolvation (typically through water desorption) overcoming a barrier of 33 kJ·mol^{-1} followed by (ii) adsorption with a barrier of 36 kJ·mol^{-1}. Once ethanol is chemisorbed at the γ-

Al_2O_3(110)/water interface, its solvation may again vary (from $CV_{solv} = 4$ to $CV_{solv} = 3$ or 5), overcoming a barrier of around 35 kJ·mol^{-1}. This confirms that *solvation* plays a key role in controlling the free energy barrier to overcome upon adsorption/desorption of ethanol at the water/alumina interface.

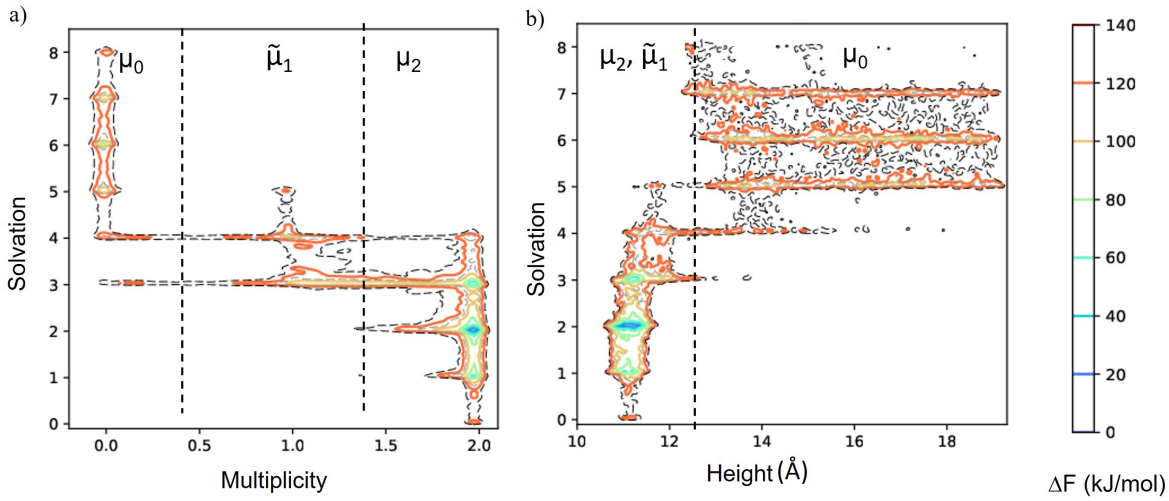

Figure 5: 2D representations of the free energy surface FES_2 built using well-tempered metadynamics starting from μ_2, with the ethanol chemisorbed dissociatively at the γ-Al_2O_3(110)/water interface. **(a)** FES_2 as a function of CV_{multi} and CV_{solv} **(b)** FES_2 as a function of CV_{height} and CV_{solv}. The macro-states μ_0 ($CV_{multi} < 0.5$, $CV_{height} > 12.5$Å, desorbed ethanol), $\tilde{\mu}_1$ ($1.5 > CV_{multi} > 0.5$, $CV_{height} < 12.5$ Å, monodentate chemisorbed ethanol) and μ_2 ($CV_{multi} > 1.5$, $CV_{height} < 12.5$ Å, bidentate chemisorbed ethanol) are separated by dash lines. Dash contour lines were added at +110 and +130 kJ·mol^{-1} to better identify the transition regions. The third collective variable has been integrated out with PLUMED.[75]

Starting from the bridging dissociative adsorption mode μ_2, well-tempered metadynamics resulted in the free energy surface FES_2 represented in Figure 5. FES_2 can be divided into three portions: the bridging ethoxy μ_2, the $\tilde{\mu}_1$ state where only one Al-O bond still connects the ethanol to the surface, and the desorbed state μ_0. It is important to note that the collective variables differ from the ones used to build FES_1. Here, $\tilde{\mu}_1$ covers a wider diversity of structures than μ_1 since Al(2) but also Al(1) are involved (see Figure 1 b)). Besides, the position of the μ_0 state is shifted by +1 along the CV_{solv} variable in FES_2 because the *solvation* has been adapted to the ethoxy case (see section 2.5.3).

Similarly to FES_1, the two chemisorbed states (μ_2 and $\tilde{\mu}_1$) correspond to a smaller volume of the phase space (10.5 Å <CV_{height}< 12.5 Å) than the desorbed state μ_0 (from 12.5 Å to 19 Å). A barrier of $\Delta F^{\ddagger}_{ads} = 46$ kJ·mol^{-1} was found, associated with an adsorption free energy of $\Delta F_{ads} = -74$ kJ·mol^{-1}(see Figure S3 b) for the corresponding 1D profile along CV_{multi}). In agreement with the thermodynamic integration and the MMSolv static method, μ_2 is once again found to be more strongly chemisorbed than μ_1. Like for μ_1, the adsorption/desorption process for μ_2 is accompanied by variations in *solvation*. In its most stable configuration, μ_2 has a *solvation* of $CV_{solv} = 2$. This *solvation* needs to increase to 3 to reach $\tilde{\mu}_1$ and then to 6 to transit to the most stable μ_0 configuration. These two successive increases correspond to the protonation of ethoxy but also to the hydration of the two aluminium Al(1) and Al(2) and the formation of the solvation sphere of ethanol. The most demanding step is the increase of CV_{solv} in μ_2, with a barrier of 98 kJ·mol^{-1}, which likely controls the kinetic of desorption process. Then, a barrier of 42 kJ·mol^{-1} needs to be overcome in $\tilde{\mu}_1$ (CV_{solv} increases from 3 to 4). In μ_0, barriers related to changes in *solvation* range 15-30 kJ·mol^{-1}.

3.4 Comparing methods

Figure 6 gathers the energetic data for the adsorption of ethanol at the γ-Al_2O_3(110)/water interface, comparing three approaches that describe explicitly water molecules up to the bulk: (i) MMSolv static method (ii) thermodynamic integration using CV_{height} as a proxy for the reaction coordinate (iii) 3D *ab initio* well-tempered metadynamics.

All three methods agree that the adsorption of ethanol at the γ-Al_2O_3(110)/water interface is exergonic and that the μ_2 adsorption mode is more stable than the μ_1 adsorption mode. This ordering is already found in absence of water as a solvent (see Figure 2a) but is amplified by the hydration (Figure 2c). The enhanced AIMD methods also predict that a barrier needs to be overcome during the adsorption process. This barrier is larger by around 10 kJ·mol^{-1}to reach the μ_2 adsorption mode than the μ_1. Besides, the barriers

obtained by thermodynamics integration are systematically lower than the ones obtained using *ab initio* metadynamics. This is likely related to *solvation* since the changes in hydration are considered to be much faster than the desorption/adsorption in the TI while these changes are sampled in the 3D *ab initio* metadynamics with the CV_{solv} variable.

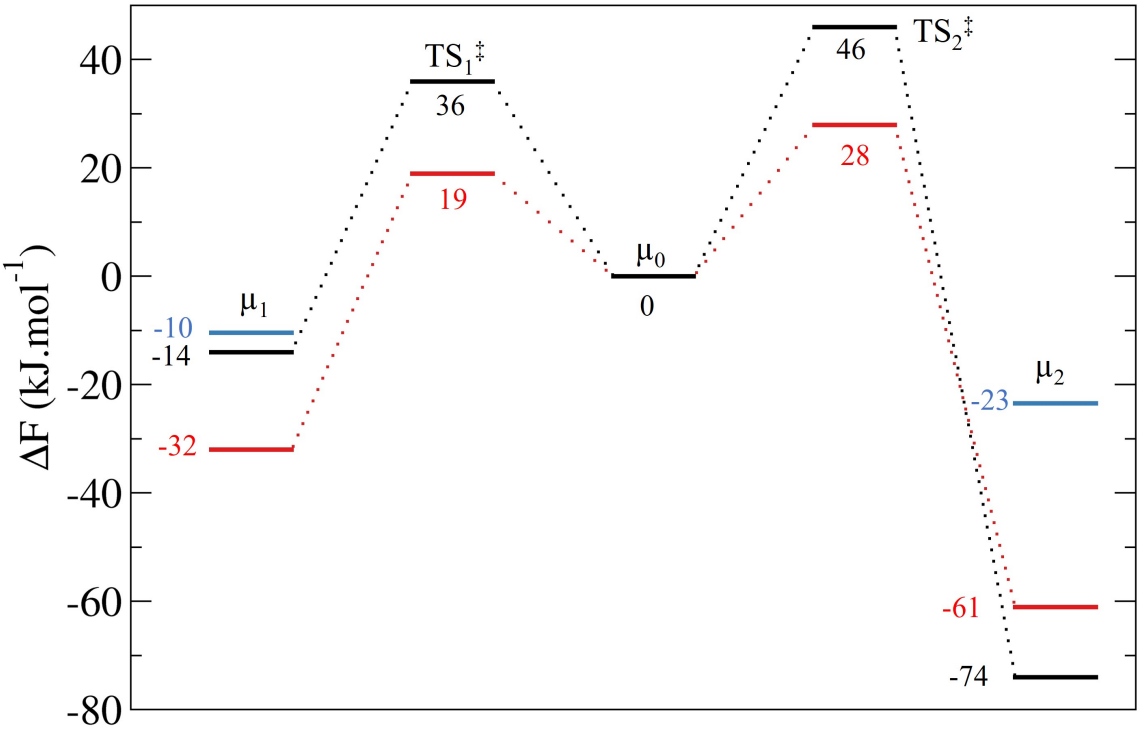

Figure 6: Free energy levels ΔF computed with well tempered metadynamics (in black), thermodynamic integration (in red) and MMSolv (in blue) for the desorption from μ_2, and μ_1.

4 Conclusion

The adsorption of ethanol at the γ-alumina/water interface was investigated comparing several computational methods. They all share the same level of theory to evaluate the interaction energy of ethanol with the surface (using PBE+D3 as a DFT functional) but they include the solvation with an increasing complexity from a polarisable continuum model to our hybrid scheme MMSolv and enhanced *ab initio* molecular dynamics (thermodynamic

integration, well-tempered metadynamics).

We compared two possible adsorption modes : (i) ethanol is kept intact and it interacts with only one aluminium atom (μ_1), (ii) ethanol is dissociated and the corresponding ethoxy bridges two aluminium atoms (μ_2). The second one has been almost systematically found to be the most stable one (except when using PCM) by at least 13 kJ·mol^{-1}, with a higher energy barrier for adsorption (10 kJ·mol^{-1} higher than for μ_1).

When using thermodynamic integration (TI), one variable was biased and all the water molecules were explicitly described and free to move. We made the hypothesis that the modification in the water structuring is faster and decoupled from the adsorption/desorption process that was described biasing the height of the ethanol as the natural reaction coordinate. Still, desorption of ethanol involves necessarily an exchange with a water molecule that will replace the chemisorbed ethanol. This replacement could not be attained in the time frame of the constrained trajectory (<20 ps). In absence of a bias to trigger the changes in solvation shells, a water molecule was brought closer to the vacant surface site using a slow growth simulation.

Well-tempered metadynamics allows to bias three collective variables for a similar computational cost as TI. Besides the height, a variable able to describe changes in solvation was included along with a variable to determine the number of Al$-$O$_{\text{ethanol}}$ bonds. This allows to determine the adsorption barrier more accurately, including the changes in the hydration shells of the surface and of the molecule (here ethanol), the proton transfers etc. Metadynamics systematically found an adsoprtion barrier greater than thermodynamic integration by around 15 kJ·mol^{-1}, a difference that is likely accounting for solvation reorganisation. This underestimation of the adsorption barrier propagates along the TI profile and may be at the origin of the larger adsorption energy found in μ_1 in comparison with MMSolv and *ab initio* metadynamics that agree on an adsorption energy of about -10 kJ·mol^{-1}.

Studying the dissociative bridging chemisorption mode μ_2 is extremely challenging.

This process not only includes an exchange between ethanol and a water molecule, but also proton transfers and likely a strong reorganisation of the localisation of the proton at the interface. Despite the extensive sampling achieved by a 3D metadynamics, no clear minimum was found for a μ_1 type chemisorption with only one $Al-O_{ethanol}$ bond and a protonated hydroxyl. This direct desorption mechanism is accompanied with a very large desorption barrier and a strongly stabilised chemisorbed μ_2 (-74 kJ·mol^{-1}). This very large stability is not in agreement with what has been found using MMsolv (-23 kJ·mol^{-1}). It is currently hard to assign the origin of the discrepancy that could be related either to insufficient sampling of the protonation configuration or missing solvation contributions in MMSolv (lack of multi-body interactions) or a missing coordinate in the set of collective variables to bias an interfacial reorganisation in AIMD.

Still, we evidenced a strong influence of the water hydration on adsorption/desorption of alcohol at the alumina/water interface. The detailed adsorption/desorption mechanism can be tackled using *ab initio* well-tempered metadynamics rather than thermodynamics integration using appropriate collective variables. Last, when screening for the most stable adsorption modes, static methods can be used including a screening of the proton localisation and the solvation using MMSolv.

Acknowledgement

This work is part of the "RatiOnAl Design for CATalysis" (ROAD4CAT) industrial chair, project IDEXLYON funded by the French National Research Agency (ANR-16-IDEX-0005) and the Commissariat-General for Investment (CGI) within the framework of Investissements d'Avenir program ("Investment for the future"). The authors thank the SYSPROD project and AXELERA Pôle de Compétitivité for financial support (PSMN Data Center). This work was also granted access to the HPC resources of CINES and IDRIS under the allocation 0800609 made by GENCI. JR and CM thank Pascal Raybaud for his insight-

ful discussions on alumina. PC and CM thank thank Alessadro Laio for his insightful discussions on collective variables.

Supporting Information Available

Most stable structures found using the static approaches (Figure and POSCAR files). Thermodynamic integrations data (cumulative error, free energy gradient, the standard error on the mean values of the fre energy gradient). Figures showing the decomposition analysis of the collective variables evolution during the TI. 1D profiles extracted from the metadynamics. Representative structures of μ_1 and μ_2 in .xyz format. Typical input files of a TI and for each well-tempered metadynamics. Trajectories and HILLS files from the two metadynamics.

References

(1) Shenghua, L.; He, Y.; Yuansheng, J. Lubrication Chemistry Viewed from DFT-Based Concepts and Electronic Structural Principles. *Int. J. Mol. Sci.* **2003**, *5*, 13.

(2) Pirkanniemi, K.; Sillanpää, M. Heterogeneous water phase catalysis as an environmental application: a review. *Chemosphere* **2002**, *48*, 1047–1060.

(3) Akpa, B. S.; D'Agostino, C.; Gladden, L. F.; Hindle, K.; Manyar, H.; McGregor, J.; Li, R.; Neurock, M.; Sinha, N.; Stitt, E. H. et al. Solvent effects in the hydrogenation of 2-butanone. *J. Catal.* **2012**, *289*, 30–41.

(4) Seh, Z. W.; Kibsgaard, J.; Dickens, C. F.; Chorkendorff, I.; Nørskov, J. K.; Jaramillo, T. F. Combining theory and experiment in electrocatalysis: Insights into materials design. *Science* **2017**, *355*, eaad4998.

(5) Verdaguer, A.; Sacha, G. M.; Bluhm, H.; Salmeron, M. Molecular Structure of Water at Interfaces: Wetting at the Nanometer Scale. *Chem. Rev.* **2006**, *106*, 1478–1510.

(6) Maier, S.; Salmeron, M. How Does Water Wet a Surface? *Acc. Chem. Res.* **2015**, *48*, 2783–2790.

(7) Björneholm, O.; Hansen, M. H.; Hodgson, A.; Liu, L.-M.; Limmer, D. T.; Michaelides, A.; Pedevilla, P.; Rossmeisl, J.; Shen, H.; Tocci, G. et al. Water at Interfaces. *Chem. Rev.* **2016**, *116*, 7698–7726.

(8) Schiros, T.; Andersson, K. J.; Pettersson, L. G. M.; Nilsson, A.; Ogasawara, H. Chemical bonding of water to metal surfaces studied with core-level spectroscopies. *J. Electron Spectrosc. Relat. Phenom.* **2010**, *177*, 85–98.

(9) Velasco-Velez, J.-J.; Wu, C. H.; Pascal, T. A.; Wan, L. F.; Guo, J.; Prendergast, D.; Salmeron, M. The structure of interfacial water on gold electrodes studied by x-ray absorption spectroscopy. *Science* **2014**, *346*, 831–834.

(10) Toney, M. F.; Howard, J. N.; Richer, J.; Borges, G. L.; Gordon, J. G.; Melroy, O. R.; Wiesler, D. G.; Yee, D.; Sorensen, L. B. Voltage-dependent ordering of water molecules at an electrode–electrolyte interface. *Nature* **1994**, *368*, 444–446.

(11) Michel, C.; Gallezot, P. Why Is Ruthenium an Efficient Catalyst for the Aqueous-Phase Hydrogenation of Biosourced Carbonyl Compounds? *ACS Catal.* **2015**, *5*, 4130–4132.

(12) Calvin, J. J.; Rosen, P. F.; Ross, N. L.; Navrotsky, A.; Woodfield, B. F. Review of surface water interactions with metal oxide nanoparticles. *J. Mater. Res.* **2019**, *34*, 416–427.

(13) Foucaud, Y.; Badawi, M.; Filippov, L. O.; Filippova, I. V.; Lebègue, S. Surface Properties of Fluorite in Presence of Water: An Atomistic Investigation. *J. Phys. Chem. B* **2018**, *122*, 6829–6836.

(14) Walsh, T. R. Pathways to Structure-Property Relationships of Peptide-Materials Interfaces: Challenges in Predicting Molecular Structures. *Acc. Chem. Res.* **2017**, *50*, 1617–1624.

(15) Leung, K.; Criscenti, L. J.; Knight, A. W.; Ilgen, A. G.; Ho, T. A.; Greathouse, J. A. Concerted Metal Cation Desorption and Proton Transfer on Deprotonated Silica Surfaces. *J. Phys. Chem. Lett.* **2018**, *9*, 5379–5385.

(16) Saleheen, M.; Heyden, A. Liquid-Phase Modeling in Heterogeneous Catalysis. *ACS Catal.* **2018**, *8*, 2188–2194.

(17) Réocreux, R.; Jiang, T.; Iannuzzi, M.; Michel, C.; Sautet, P. Structuration and Dynamics of Interfacial Liquid Water at Hydrated γ-Alumina Determined by ab Initio Molecular Simulations: Implications for Nanoparticle Stability. *ACS Appl. Nano Mater.* **2018**, *1*, 191–199.

(18) Wright, L. B.; Walsh, T. R. Facet Selectivity of Binding on Quartz Surfaces: Free Energy Calculations of Amino-Acid Analogue Adsorption. *J. Phys. Chem. C* **2012**, *116*, 2933–2945.

(19) Ali, A.; Le, T. T. B.; Striolo, A.; Cole, D. R. Salt Effects on the Structure and Dynamics of Interfacial Water on Calcite Probed by Equilibrium Molecular Dynamics Simulations. *J. Phys. Chem. C* **2020**, *124*, 24822–24836.

(20) Faheem, M.; Heyden, A. Hybrid Quantum Mechanics/Molecular Mechanics Solvation Scheme for Computing Free Energies of Reactions at Metal–Water Interfaces. *J. Chem. Theory Comput.* **2014**, *10*, 3354–3368.

(21) Steinmann, S. N.; Sautet, P.; Michel, C. Solvation free energies for periodic surfaces: comparison of implicit and explicit solvation models. *Phys. Chem. Chem. Phys.* **2016**, *18*, 31850–31861.

(22) Lim, H.-K.; Lee, H.; Kim, H. A Seamless Grid-Based Interface for Mean-Field QM/MM Coupled with Efficient Solvation Free Energy Calculations. *J. Chem. Theory Comput.* **2016**, *12*, 5088–5099.

(23) Naserifar, S.; Chen, Y.; Kwon, S.; Xiao, H.; Goddard, W. A. Artificial Intelligence and QM/MM with a Polarizable Reactive Force Field for Next-Generation Electrocatalysts. *Matter* **2021**, *4*, 195–216.

(24) Zhang, X.; DeFever, R. S.; Sarupria, S.; Getman, R. B. Free Energies of Catalytic Species Adsorbed to Pt(111) Surfaces under Liquid Solvent Calculated Using Classical and Quantum Approaches. *J. Chem. Inf. Model.* **2019**, *59*, 2190–2198, PMID: 30821458.

(25) Clabaut, P.; Schweitzer, B.; Götz, A. W.; Michel, C.; Steinmann, S. N. Solvation Free Energies and Adsorption Energies at the Metal/Water Interface from Hybrid Quantum-Mechanical/Molecular Mechanics Simulations. *J. Chem. Theory Comput.* **2020**, *16*, 6539–6549.

(26) Blanck, S.; Martí, C.; Loehlé, S.; Steinmann, S. N.; Michel, C. (Dis)Similarities of adsorption of diverse functional groups over alumina and hematite depending on the surface state. *J. Chem. Phys.* **2021**, *154*, 084701.

(27) Li, C.; Monti, S.; Carravetta, V. Journey toward the Surface: How Glycine Adsorbs on Titania in Water Solution. *J. Phys. Chem. C* **2012**, *116*, 18318–18326.

(28) Raju, M.; Kim, S.-Y.; van Duin, A. C. T.; Fichthorn, K. A. ReaxFF Reactive Force Field Study of the Dissociation of Water on Titania Surfaces. *J. Phys. Chem. C* **2013**, *117*, 10558–10572.

(29) Hahn, S. H.; van Duin, A. C. T. Surface Reactivity and Leaching of a Sodium Silicate Glass under an Aqueous Environment: A ReaxFF Molecular Dynamics Study. *J. Phys. Chem. C* **2019**, *123*, 15606–15617.

(30) Zhao, Y. L.; Köppen, S.; Frauenheim, T. An SCC-DFTB/MD Study of the Adsorption of Zwitterionic Glycine on a Geminal Hydroxylated Silica Surface in an Explicit Water Environment. *J. Phys. Chem. C* **2011**, *115*, 9615–9621.

(31) Spiegelman, F.; Tarrat, N.; Cuny, J.; Dontot, L.; Posenitskiy, E.; Martí, C.; Simon, A.; Rapacioli, M. Density-functional tight-binding: basic concepts and applications to molecules and clusters. *Acv. Phys. X* **2020**, *5*, 1710252.

(32) Artrith, N.; Kolpak, A. M. Understanding the Composition and Activity of Electrocatalytic Nanoalloys in Aqueous Solvents: A Combination of DFT and Accurate Neural Network Potentials. *Nano Lett.* **2014**, *14*, 2670–2676.

(33) Behler, J. Constructing high-dimensional neural network potentials: A tutorial review. *Int. J. Quantum Chem.* **2015**, *115*, 1032–1050.

(34) Natarajan, S. K.; Behler, J. Neural network molecular dynamics simulations of solid–liquid interfaces: water at low-index copper surfaces. *Phys. Chem. Chem. Phys.* **2016**, *18*, 28704–28725.

(35) Laio, A.; Parrinello, M. Escaping free-energy minima. *PNAS* **2002**, *99*, 12562–12566.

(36) Laio, A.; Gervasio, F. L. Metadynamics: a method to simulate rare events and reconstruct the free energy in biophysics, chemistry and material science. *Rep. Prog. Phys.* **2008**, *71*, 126601.

(37) Liu, L.-M.; Laio, A.; Michaelides, A. Initial stages of salt crystal dissolution determined with ab initio molecular dynamics. *Phys. Chem. Chem. Phys.* **2011**, *13*, 13162.

(38) Schneider, J.; Colombi Ciacchi, L. Specific Material Recognition by Small Peptides Mediated by the Interfacial Solvent Structure. *J. Am. Chem. Soc.* **2012**, *134*, 2407–2413.

(39) Käner, J. Umbrella sampling. *WIREs Comput. Mol. Sci.* **2011**, *1*, 932–942.

(40) Tazi, S.; Rotenberg, B.; Salanne, M.; Sprik, M.; Sulpizi, M. Absolute acidity of clay edge sites from ab-initio simulations. *Geochim. Cosmochim. Acta* **2012**, *94*, 1–11.

(41) Parashar, S.; Lesnicki, D.; Sulpizi, M. Increased Acid Dissociation at the Quartz/Water Interface. *J. Phys. Chem. Lett.* **2018**, *9*, 2186–2189.

(42) Bailleul, S.; Rogge, S. M. J.; Vanduyfhuys, L.; Van Speybroeck, V. Insight into the Role of Water on the Methylation of Hexamethylbenzene in H-SAPO-34 from First Principle Molecular Dynamics Simulations. *ChemCatChem* **2019**, *11*, 3993–4010.

(43) Michaelis, M.; Delle Piane, M.; Rothenstein, D.; Perry, C. C.; Colombi Ciacchi, L. Lessons from a Challenging System: Accurate Adsorption Free Energies at the Amino Acid/ZnO Interface. *J. Chem. Theory Comput.* **2021**, *17*, 4420–4434.

(44) Ravenelle, R. M.; Copeland, J. R.; Van Pelt, A. H.; Crittenden, J. C.; Sievers, C. Stability of Pt/γ-Al_2O_3 Catalysts in Model Biomass Solutions. *Top. Catal.* **2012**, *55*, 162–174.

(45) Réocreux, R.; Girel, E.; Clabaut, P.; Tuel, A.; Besson, M.; Chaumonnot, A.; Cabiac, A.; Sautet, P.; Michel, C. Reactivity of shape-controlled crystals and metadynamics simulations locate the weak spots of alumina in water. *Nat. Commun.* **2019**, *10*, 3139.

(46) Copeland, J. R.; Shi, X.-R.; Sholl, D. S.; Sievers, C. Surface Interactions of C $_2$ and C $_3$ Polyols with γ-Al_2 O_3 and the Role of Coadsorbed Water. *Langmuir* **2013**, *29*, 581–593.

(47) Copeland, J. R.; Santillan, I. A.; Schimming, S. M.; Ewbank, J. L.; Sievers, C. Surface Interactions of Glycerol with Acidic and Basic Metal Oxides. *J. Phys. Chem. C* **2013**, *117*, 21413–21425, Publisher: American Chemical Society.

(48) Krokidis, X.; Raybaud, P.; Gobichon, A. E.; Rebours, B.; Euzen, P.; Toulhoat, H. Theoretical study of the dehydration process of boehmite to gamma-alumina. *J. Phys. Chem. B* **2001**, *105*, 5121–5130.

(49) Digne, M.; Sautet, P.; Raybaud, P.; Euzen, P.; Toulhoat, H. Hydroxyl Groups on γ-Alumina Surfaces: A DFT Study. *J. Catal.* **2002**, *211*, 1–5.

(50) Wischert, R.; Laurent, P.; Coperet, C.; Delbecq, F.; Sautet, P. gamma-Alumina: The Essential and Unexpected Role of Water for the Structure, Stability, and Reactivity of "Defect" Sites. *J. Am. Chem. Soc.* **2012**, *134*, 14430–14449.

(51) Kresse, G. Ab initio molecular dynamics for liquid metals. *J. Non-Cryst. Solids* **1995**, *192-193*, 222–229.

(52) Kresse, G.; Furthmüller, J. Efficient iterative schemes for *ab initio* total-energy calculations using a plane-wave basis set. *Phys. Rev. B* **1996**, *54*, 11169–11186.

(53) Perdew, J. P.; Wang, Y. Accurate and simple analytic representation of the electron-gas correlation energy. *Phys. Rev. B* **1992**, *45*, 13244–13249.

(54) Perdew, J. P.; Burke, K.; Ernzerhof, M. Generalized Gradient Approximation Made Simple. *Phys. Rev. Lett.* **1996**, *77*, 3865–3868.

(55) Steinmann, S. N.; Corminboeuf, C. Comprehensive Benchmarking of a Density-Dependent Dispersion Correction. *J. Chem. Theory Comput.* **2011**, *7*, 3567–3577.

(56) Gautier, S.; Steinmann, S. N.; Michel, C.; Fleurat-Lessard, P.; Sautet, P. Molecular adsorption at Pt(111). How accurate are DFT functionals? *Phys. Chem. Chem. Phys.* **2015**, *17*, 28921.

(57) Blochl, P. E. Projector augmented-wave method. *Phys. Rev. B* **1994**, *50*, 17953.

(58) Kresse, G.; Joubert, D. From ultrasoft pseudopotentials to the projector augmented-wave method. *Phys. Rev. B* **1999**, *59*, 1758–1775.

(59) Mathew, K.; Sundararaman, R.; Letchworth-Weaver, K.; Arias, T. A.; Hennig, R. G. Implicit solvation model for density-functional study of nanocrystal surfaces and reaction pathways. *J. Chem. Phys.* **2014**, *140*, 084106.

(60) Wertz, D. H. Relationship between the gas-phase entropies of molecules and their entropies of solvation in water and 1-octanol. *J. Am. Chem. Soc.* **1980**, *102*, 5316–5322.

(61) Skelton, A. A.; Fenter, P.; Kubicki, J. D.; Wesolowski, D. J.; Cummings, P. T. Simulations of the Quartz$(10\bar{1}1)$/Water Interface: A Comparison of Classical Force Fields, Ab Initio Molecular Dynamics, and X-ray Reflectivity Experiments. *J. Phys. Chem. C* **2011**, *115*, 2076–2088.

(62) Rappe, A. K.; Casewit, C. J.; Colwell, K. S.; Goddard, W. A.; Skiff, W. M. UFF, a full periodic table force field for molecular mechanics and molecular dynamics simulations. *J. Am. Chem. Soc.* **1992**, *114*, 10024–10035.

(63) VandeVondele, J.; Krack, M.; Mohamed, F.; Parrinello, M.; Chassaing, T.; Hutter, J. QUICKSTEP: Fast and accurate density functional calculations using a mixed Gaussian and plane waves approach. *Comput. Phys. Commun.* **2005**, *167*, 103–128.

(64) VandeVondele, J.; Hutter, J. Gaussian basis sets for accurate calculations on molecular systems in gas and condensed phases. *J. Chem. Phys.* **2007**, *127*, 114105.

(65) Lippert, G.; Hutter, J.; Parrinello, M. A hybrid Gaussian and plane wave density functional scheme. *Mol. Phys.* **1997**, *92*, 477–487.

(66) Hutter, J.; Iannuzzi, M.; Schiffmann, F.; VandeVondele, J. CP2K: atomistic simulations of condensed matter systems. *WIREs Comput. Mol. Sci.* **2014**, *4*, 15–25.

(67) Goedecker, S.; Teter, M.; Hutter, J. Separable dual-space Gaussian pseudopotentials. *Phys. Rev. B* **1996**, *54*, 1703–1710.

(68) Hartwigsen, C.; Goedecker, S.; Hutter, J. Relativistic separable dual-space Gaussian pseudopotentials from H to Rn. *Phys. Rev. B* **1998**, *58*, 3641–3662.

(69) Krack, M. Pseudopotentials for H to Kr optimized for gradient-corrected exchange-correlation functionals. *Theor. Chem. Acc.* **2005**, *114*, 145–152.

(70) Grimme, S.; Antony, J.; Ehrlich, S.; Krieg, H. A consistent and accurate *ab initio* parametrization of density functional dispersion correction (DFT-D) for the 94 elements H-Pu. *J. Chem. Phys.* **2010**, *132*, 154104.

(71) Bussi, G.; Donadio, D.; Parrinello, M. Canonical sampling through velocity rescaling. *J. Chem. Phys.* **2007**, *126*, 014101.

(72) Tuckerman, M. E. *Statistical Mechanics: Theory and Molecular Simulation*; Oxford University Press, 2010.

(73) Barducci, A.; Bussi, G.; Parrinello, M. Well-Tempered Metadynamics: A Smoothly Converging and Tunable Free-Energy Method. *Phys. Rev. Lett.* **2008**, *100*, 020603.

(74) Bonomi, M.; Bussi, G.; Camilloni, C.; Tribello, G. A.; Banáš, P.; Barducci, A.; Bernetti, M.; Bolhuis, P. G.; Bottaro, S.; Branduardi, D. et al. Promoting transparency and reproducibility in enhanced molecular simulations. *Nat. Methods* **2019**, *16*, 670–673.

(75) Tribello, G. A.; Bonomi, M.; Branduardi, D.; Camilloni, C.; Bussi, G. PLUMED 2: New feathers for an old bird. *Comput. Phys. Commun.* **2014**, *185*, 604–613.

(76) Raiteri, P.; Laio, A.; Gervasio, F. L.; Micheletti, C.; Parrinello, M. Efficient Reconstruction of Complex Free Energy Landscapes by Multiple Walkers Metadynamics. *J. Phys. Chem. B* **2006**, *110*, 3533–3539.

(77) Gray, C. M.; Saravanan, K.; Wang, G.; Keith, J. A. Quantifying solvation energies at solid/liquid interfaces using continuum solvation methods. *Mol. Simul.* **2017**, *43*, 420–427.

(78) Zhang, Q.; Asthagiri, A. Solvation effects on DFT predictions of ORR activity on metal surfaces. *Catal. Today* **2019**, *323*, 35–43.

(79) Rendón-Calle, A.; Builes, S.; Calle-Vallejo, F. Substantial improvement of electrocatalytic predictions by systematic assessment of solvent effects on adsorption energies. *Appl. Catal., B* **2020**, *276*, 119147.

Graphical TOC Entry